A&A 367, 1033–1048 (2001)
DOI: 10.1051/0004-6361:20000495

Astronomy & Astrophysics

Influence of magnetic fields on the coherence effects in the Na I D_1 and D_2 lines

J. O. Stenflo[1], A. Gandorfer[1], T. Wenzler[1], and C. U. Keller[2]

[1] Institute of Astronomy, ETH Zentrum, 8092 Zurich, Switzerland
[2] National Solar Observatory, PO Box 26732, Tucson, AZ 85726-6732, USA

Received 1 September 2000 / Accepted 12 December 2000

Abstract. To clarify the physical nature of the enigmatic scattering polarization in the Na I D_1 and D_2 line cores we have explored their behavior with full Stokes vector polarimetry in regions with varying degree of magnetic activity near the solar limb. These observations represent the first time that ZIMPOL II, the second generation of our CCD based imaging polarimeter systems, has been used for a scientific program. With ZIMPOL II the four Stokes images can be demodulated and recorded with a single CCD sensor such that the resulting images of the fractional polarization Q/I, U/I, and V/I are entirely free from spurious features due to seeing or flat-field effects. The polarization in the cores of the lines, in particular in D_2, exhibits dramatic and unexpected spatial variations in both Q/I and U/I, including polarization self-reversals of the D_2 Q/I core peak. As the fluctuations in the Q, U, and V parameters appear to be relatively uncorrelated, we have parametrized the profiles and made scatter plots of the extracted parameters. Comparison with synthetic scatter plots based on different theoretical models suggests that the polarization signals in the cores of the D_2 and D_1 lines have different physical origins: While the D_1 core is likely to be governed by ground-state atomic polarization, the D_2 core is dominated by the alignment of the excited state and by effects of partial frequency redistribution.

Key words. polarization – scattering – Sun: magnetic fields – atomic processes – techniques: polarimetric

1. Introduction

The so-called "second solar spectrum", the linearly polarized spectrum that is produced by coherent scattering processes, is full of anomalous features that have so far defied theoretical explanations (Stenflo et al. 2000b). The probably most conspicuous of these features is the complex polarization profile across the Na I D_1 5895.94 and D_2 5889.97 Å lines. The relatively large polarization amplitudes in these lines make them well accessible to detailed analysis (Stenflo et al. 1980, 1983, 2000a; Stenflo & Keller 1996, 1997). While the polarization outside the central cores of the Na I D_1 and D_2 lines has been successfully explained in terms of quantum-mechanical interference between the $J = \frac{3}{2}$ and $\frac{1}{2}$ fine-structure components of the upper states of the D_2 and D_1 lines (Stenflo 1980), the narrow but pronounced core peaks have remained enigmatic.

The first (and so far only) rather convincing explanation for these core peaks was proposed by Landi Degl'Innocenti (1998, 1999) in terms of lower-level atomic polarization. Due to hyperfine structure splitting, the normally unpolarizable $J = \frac{1}{2}$ ground state gets split into components with new total angular momentum quantum numbers F. These hyperfine structure states can acquire atomic polarization by an optical pumping process: atomic alignment is first induced in the excited state by the anisotropic excitation. By subsequent spontaneous radiative decay there is a transfer of some of this alignment to the ground state. Many such processes lead to a statistical equilibrium with an aligned ground state.

The main problem with this explanation is however the extreme vulnerability of the ground state alignment to depolarization by magnetic fields and collisions. As the life time of the ground state (mainly determined by the time beween two radiative excitations) is for typical conditions in the solar atmosphere about two orders of magnitude larger than the life time of the excited state (determined by the spontaneous decay rate), the ground state will be depolarized by magnetic fields that are two orders of magnitude weaker than those needed to depolarize the excited state. This follows because the field sensitivity according to the Hanle effect is determined by the ratio between the life time of the atomic state and the Larmor precession period. For the explanation in terms of lower-level polarization to work, the Sun's magnetic field would need to be either unacceptably weak ($\lesssim$10 mG according to Landi Degl'Innocenti), or its orientation would need to be close to vertical, since when the illumination of the scattering

Send offprint requests to: J. O. Stenflo,
e-mail: stenflo@astro.phys.ethz.ch

particle is symmetric around the magnetic field vector (as it would in general be for a vertical field), the Hanle effect vanishes. However, in the lower chromosphere, where the cores of the D_2 and D_1 lines are formed, the magnetic field is expected to be highly inclined and canopy-like (Giovanelli 1980; Jones & Giovanelli 1983). Furthermore, Hanle effect observations in other lines provide evidence for the ubiquitous presence of magnetic fields that are sufficiently strong to significantly depolarize the excited atomic states (Bianda et al. 1998a,b, 1999).

The previous polarimetric observations of the Na I D_1 and D_2 lines have focused on exploring the properties of the "non-magnetic" scattering polarization seen in Stokes Q/I, rather than exploring the behavior of the full Stokes vector. This has been a natural initial limitation, since we first need to study and try to understand the physics of the simplest case before we introduce the considerable complication of magnetic fields, and in the strictly "non-magnetic" case Stokes U and V should be zero for symmetry reasons. The term "non-magnetic" is used here in a relative sense, since no volume of the solar atmosphere is truly non-magnetic due to the ubiquitous nature of the magnetic field. The term simply means that we have selected the most quiet, least magnetic regions on the Sun for the observations.

Another more practical reason for the previous focus on the non-magnetic case has to do with the technical complication. The first generation of our ZIMPOL (Zurich Imaging Polarimeter, cf. Povel 1995) polarimetric system could only handle two image planes, i.e., two Stokes parameters, simultaneously, which made it impractical to use it for full vector polarimetry. It however allowed for unprecedented polarimetric accuracy, routinely to the 10^{-5} and in one long-integration case to the $5\ 10^{-6}$ level, since it was basically free from systematic effects down to this level. It must be pointed out, however, that such high sensitivities are only possible (when using high spectral resolution) in the non-magnetic case, since we can then do spatial averaging along the spectrograph slit to suppress the stochastic photon noise. In the magnetic case such averaging is usually not allowed, since solar magnetic fields are highly structured with spatial variations along the slit. There is a natural trade-off between spatial resolution and polarimetric accuracy, depending on the size (photon-collecting area) of the telescope (Stenflo 1999).

A new generation of our polarimeter system, ZIMPOL II (Stenflo et al. 1992; Stenflo 1994; Gandorfer & Povel 1997; Gandorfer 1999) is now available. A charge-shifting scheme allows four simultaneous image planes to be rapidly cycled, in the kHz range, between one exposed area and three hidden buffer storage zones within a single CCD sensor. Linear combination of the four simultaneous images give images in each of the four Stokes parameters, free from seeing and gain table noise. This allows high-precision vector polarimetry, with the achievable accuracy being limited exclusively by photon noise and instrumental polarization of the telescope used. ZIMPOL II allows us to go from the "non-magnetic" case to explore by full vector polarimetry the influence of magnetic fields on the scattering polarization. It was used for the first time for scientific programs at NSO/Kitt Peak in October 1999 and March 2000. The present paper reports on results of these observations.

With vector polarimetry and symmetry-breaking magnetic fields a new dimension is introduced in the scattering polarization problem. The way in which magnetic fields influence the line polarization via the Hanle and Zeeman effects depends on the physical processes that are responsible for the polarized emission, including the coupling to the various atomic levels with their different life times, Landé factors, and collisional sensitivities. Due to the strong spatial structuring of the magnetic field across the solar disk, the relative influence of the Hanle effect and the transverse and longitudinal Zeeman effects will fluctuate greatly, which leads to varying spectral signatures in the different Stokes parameters. The observed relative variations of the shapes of the Stokes profiles provide a rich set of qualitatively new, empirical information that will both guide and constrain future theoretical efforts. In the present paper we will present the observed magnetic-field effects on the Na I D_1 and D_2 lines and use the results to try to identify the physical processes responsible for the D_1 and D_2 core polarization peaks.

2. Observational material and data reduction techniques

All the observations reported here were made with the ZIMPOL II system attached to the McMath-Pierce facility of the National Solar Observatory (Kitt Peak) during two observing runs, in October 1999 and March 2000.

2.1. Selection of spectral lines and solar regions

Solar regions near the limb with varying degrees of magnetic activity were selected, to try to cover much of the range from weak to intermediate to strong magnetic fields. The spectrograph slit was always oriented parallel to the nearest solar limb (perpendicular to the radius vector from disk center), so that all points along the slit are at the same limb distance. Positive Stokes Q is always defined as polarization with the electric vector parallel to the slit. The field of view along the slit was about 69 arcsec. It included 97 exposed pixels rows (each of which is separated by three covered pixel rows used for fast buffer storage). The spatial step between the exposed pixel rows was 0.71 arcsec. The slit width was normally 160 μm, which corresponds to 0.4 arcsec or 31 mÅ. Most of the recordings were made at a limb distance corresponding to $\mu = 0.1$ (where μ is the cosine of the heliocentric angle), but at various position angles to sample regions of different magnetic activity. In a number of cases other limb distances were also chosen, in particular to sample regions in and around large sunspots.

Our observing program to explore the influence of magnetic fields on the scattering polarization included a

number of spectral regions, like Sr I 4607 Å, Ba II 4934, 6142, and 6497 Å, the 5165–5185 Å region around the strong Mg I lines, the three quantum-interfering fine-structure components of Cr I around 5207 Å (first observed at IRSOL; Gandorfer 2000), the 5250 Å region, Fe 5445 Å, He I D_3 5876 Å, Na I D_1 and D_2, Ca I 6103 and 6162 Å, Hα 6563 Å. An overview of this data set has been presented by Wenzler (2000). In the present paper we however limit ourselves to a discussion of the results for the Na I D_1 and D_2 system. Also, to avoid effects of center-to-limb distance, we will only consider recordings made at $\mu = 0.1$, except for one recording in a big sunspot, which is used here only to illustrate the signatures of the Zeeman effect, without scattering effects. All $\mu = 0.1$ recordings show spatially varying signatures of magnetic fields in the weak and intermediate-strength Hanle regimes, for which the linear polarization in the line core is dominated by scattering effects rather than the transverse Zeeman effect. The circular polarization on the other hand is always controlled by the longitudinal Zeeman effect, since scattering effects cannot by themselves produce circular polarization.

2.2. Removal of instrumental effects

The most serious instrumental problem is the large and time-varying telescope polarization produced by the two oblique reflections at mirrors nos. 1 (the heliostat) and 3 in the McMath-Pierce facility. We have considered three ways to deal with this problem: (1) Optical compensation of the telescope polarization; (2) Modelling of the telescope Mueller matrix, with observational calibration of the free parameters in the model; (3) Removal of cross talk between the Stokes parameters in the data analysis, making use of the known qualitative difference between the spectral signatures of the Stokes parameters.

Since no complete optical compensator that could also remove the spurious phase retardations in the system was available, a partial optical compensation of the Q and U polarizations with a tilting, plane-parallel glass plate was used during the October 1999 run. Numerical simulations of the telescope polarization (Gisler 1999) however subsequently showed that the overall properties of the telescope Mueller matrix are rather made worse by such a plate, and that a contemplated system achieving phase compensation with a Bowen compensator would also have undesirable side effects.

For the March 2000 run we therefore decided to abandon optical compensation altogether and instead explore how far one can get with detailed telescope modelling and calibration. All the telescope mirrors had been freshly aluminized immediately before our March observing run, and we devoted the full first observing day of that run to record the instrumental polarization at different wavelengths, as a function of hour angle throughout the day. These data will be used to constrain the model and fix the values of its free parameters. This modelling and exploration of the telescope properties is however outside the scope of the present paper and will be dealt with separately later.

Instead we limit ourselves here to the use of the third method listed above, removal of the cross talk in the data analysis. Although this method may in general lead to ambiguous and non-unique results, it is sufficient without any significant uniqueness problem in our special case of limb ($\mu = 0.1$) observations of the Na I D_1 and D_2 lines in regions of only weak or moderately strong magnetic fields, when the scattering polarization and Hanle signatures dominate over the transverse Zeeman effect in the linear polarization. In this case, which is the only one considered here, the spectral signatures in the Q, U, and V parameters are qualitatively entirely different, as we will see illustrated below. This fortunate situation however does not apply to vector polarimetry further from the limb, near sunspots, when the Zeeman effect dominates over the scattering polarization effects. The biggest problem in this Zeeman case is the cross talk between Q and U, since the transverse Zeeman effect has qualitatively the same signature in these two parameters. This problem does not arise for the Hanle effect.

The cross talk from Stokes I into Q, U, and V leads to a spectrally flat displacement of the zero line of the polarization scale in Q/I, U/I, and V/I. For U/I and V/I it is very easy to find the correct zero line, since we know that the intrinsic polarization in the continuum should be zero for symmetry reasons. This is not the case for Q/I, where a significant continuum polarization is present. We deal with this by shifting the Q/I spectra so that the signal asymptotically approaches the continuum polarization level determined theoretically by Fluri & Stenflo (1999) and in addition ensure that the zero crossing of the polarization curve between the D_2 and D_1 lines is consistent with theoretical modelling and previous observational work, as described in some more detail in Stenflo et al. (2000a).

In some of the recordings polarized interference fringes could be seen. Since they were very localized in the 2-D Fourier domain, they could be removed by Fourier filtering, after some experimentation to optimize the filter. 2-D wavelet smoothing has been applied to the final images. The reduction procedure has been described in detail by Wenzler (2000).

3. Examples of diverse behavior in the mixed Zeeman-Hanle regime

While the Stokes signatures of the Zeeman effect are well known, the spectral signatures of magnetic fields in the scattering polarization represent largely unexplored territory, in particular in the intermediate regime, where the Hanle and Zeeman effects mix. For the Na I D_1 and D_2 lines we cannot even refer to any established theory, since there is no consensus concerning the physical mechanisms responsible for the core polarization peaks in the D_1 and D_2 lines. It is therefore useful to first illustrate the Stokes signatures of the Zeeman effect in the absence of significant scattering polarization, and use this for

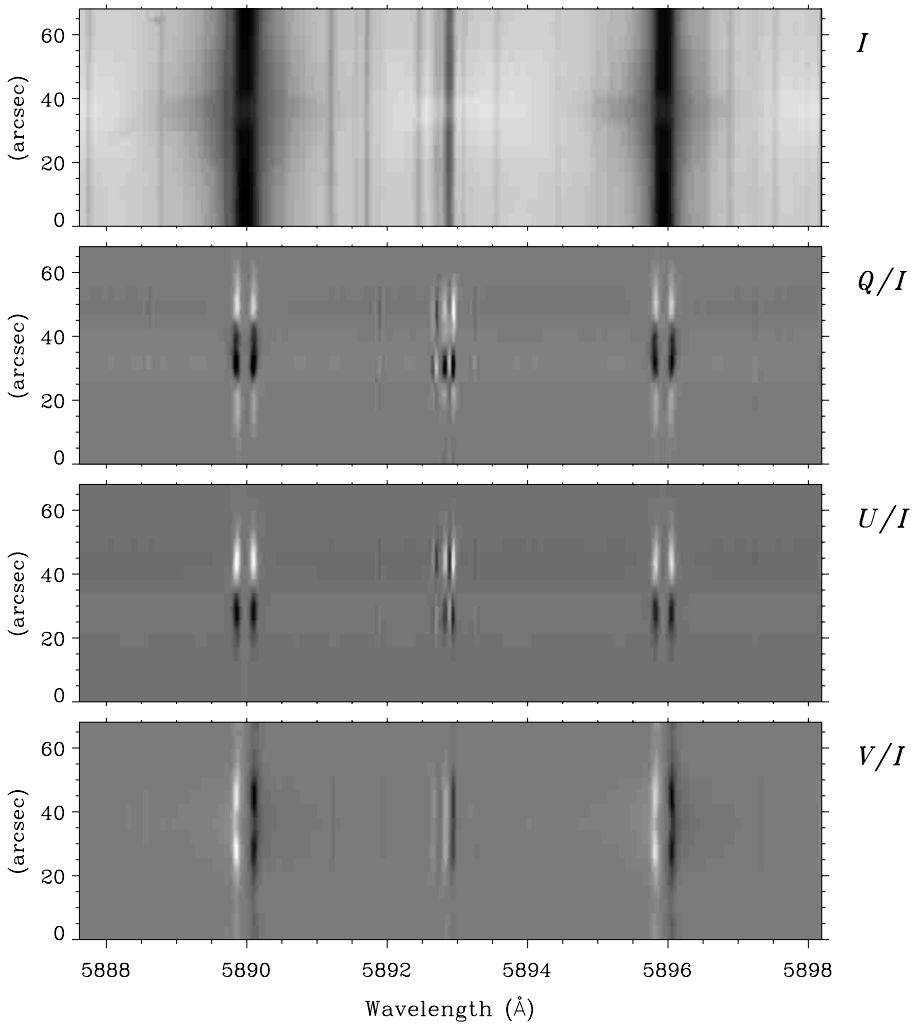

Fig. 1. Stokes spectra of a sunspot at a limb distance corresponding to $\mu = 0.43$

reference and comparison purposes when considering the magnetic effects on the scattering polarization.

For this purpose we present in Fig. 1 a recording made with the slit crossing a large sunspot at $\mu = 0.43$. Here we see the characteristic signatures of the Zeeman effect: Approximately symmetric profiles in Q and U due to the transverse Zeeman effect, anti-symmetric in V due to the longitudinal Zeeman effect. The signals in the D_2 and D_1 lines are of comparable strength. There is also a fairly strong signal from the transverse Zeeman effect in the Ni I line between the D_2 and D_1 lines. As expected, the profile shapes in Q and U are qualitatively similar. No attempt has been made here to correct for cross talk between Q and U.

As a contrast, let us now show a few examples of magnetic signatures in the scattering polarization, as recorded near the limb at $\mu = 0.1$. The recording in Fig. 2 for the first time shows prominent spatial variations of the D_2 core polarization in both Q/I and U/I, while the signal in the D_1 core remains quite weak. It is obvious from a comparison with Fig. 1 that there is no qualitative similarity at all with the transverse Zeeman effect, but that we have to do with something entirely different. There is no significant signal in the Ni I line. We also notice that the broader wing polarization in Q/I does not vary spatially, and that wing polarization is absent in U/I. This is entirely consistent with the expected behavior of the Hanle effect, since theory shows that the Hanle effect only operates in the Doppler cores but not the wings of spectral lines (Omont et al. 1973; Stenflo 1994, 1998). The anti-symmetric profiles in V/I, which show up with similar magnitudes in the D_2 and D_1 lines, are clear signatures of the longitudinal Zeeman effect, as a comparison with Fig. 1 shows.

The different Stokes parameters contain different and complementary information. The fluctuating Q/I core polarization is due to Hanle depolarization by spatially varying magnetic fields, the U/I polarization represents Hanle rotation of the plane of linear polarization due to magnetic fields whose orientation varies along the slit, while the V/I polarization due to the longitudinal Zeeman effect is a measure of the line-of-sight component of the magnetic flux. In the absence of magnetic fields U and V would be zero, while Q would remain prominent but spatially invariant (for a given limb distance).

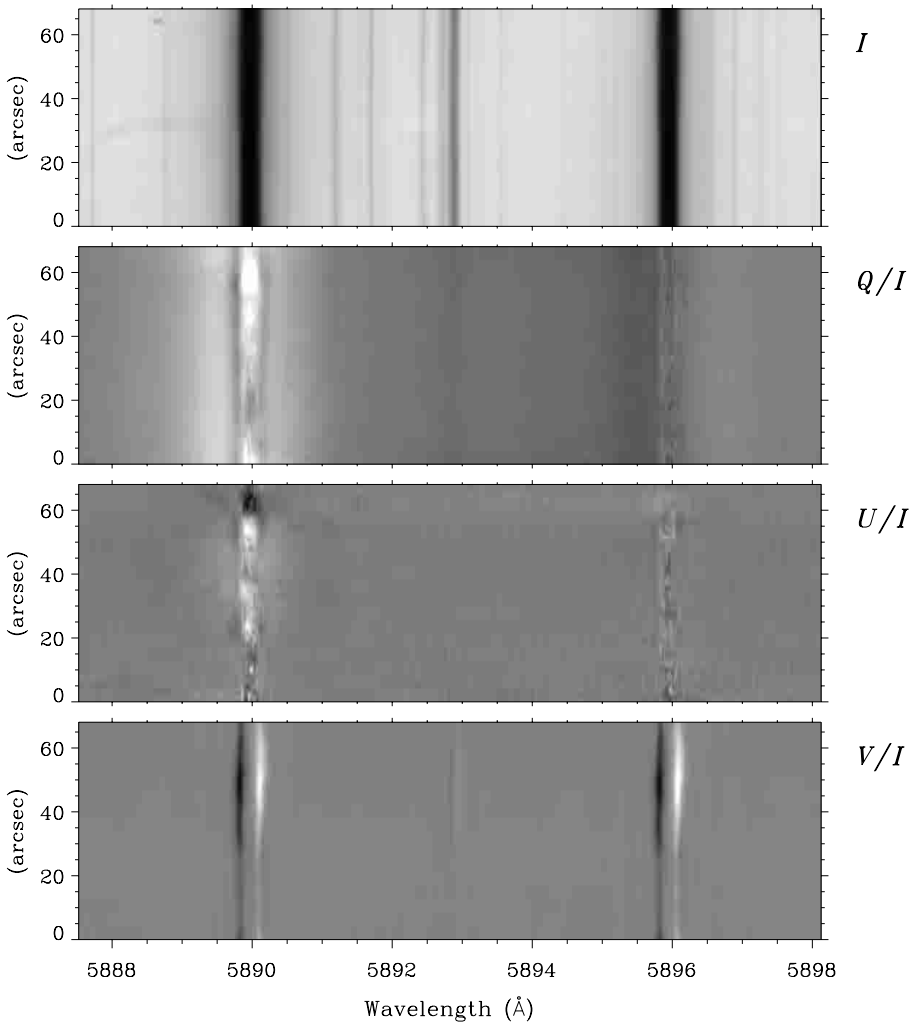

Fig. 2. Stokes spectra of a magnetic region near the SE limb at $\mu = 0.1$

One important feature in Fig. 2 that is also typical for other recordings is that there is no obvious correlation between the magnetically-induced fluctuations in the Q, U, and V parameters. This is not entirely surprising, since they respond to different properties of the magnetic field vector. We will return to this question later in connection with the theoretical interpretations.

Another example of the complex and diverse behavior of the core polarization is shown in Fig. 3. Like in Fig. 2 there is little correlation between the spatial variations in the different Stokes parameters. Notice in particular the long section of the slit where there is a strong self-reversal of the Q/I core polarization in D_2. In the middle of this slit section U/I changes sign from negative to positive.

To bring out the profile shapes better and in graphical detail we can zoom in on selected spatial sections along the slit, magnify them and plot spatial averages over the selected sections. An example of this is shown in Fig. 4, where the selected section is identified by using the same spatial scale as in Fig. 2. The scale shows that the 61–66 arcsec section was selected, i.e., the uppermost portion of Fig. 2. In this portion we have a strong, dark (negative) core feature in U/I, while Q/I has a prominent white (positive) core peak, which however is not quite cospatial with the negative U/I feature.

The upper part of Fig. 4 shows a zoomed version of the four 2-D Stokes spectra, while the lower part shows the corresponding 1-D spectral plots, obtained by spatial averaging of the 2-D spectra. The main features seen in the figure are: pronounced single-peak negative polarization in U/I in the D_2 core, while the D_1 core shows weak but significant positive polarization; Strong core peak in Q/I in the D_2 core, with almost nothing in the D_1 core; "Well-behaved" anti-symmetric V/I profiles, with some predominance of the red-wing lobes in both the D_2 and D_1 lines.

Similarly we show in Fig. 5 a zoomed-in portion of Fig. 3. We have selected the portion that avoids the sign change in U/I while still containing part of the spectacular self-reversal in Q/I. The signal in U/I is an order of magnitude smaller than in Q/I and has no polarization in the wings. V/I is anti-symmetric, but this time the blue-wing lobes dominate.

Inspection of Figs. 2–5 shows that errors due to incorrectly applied corrections for instrumental polarization

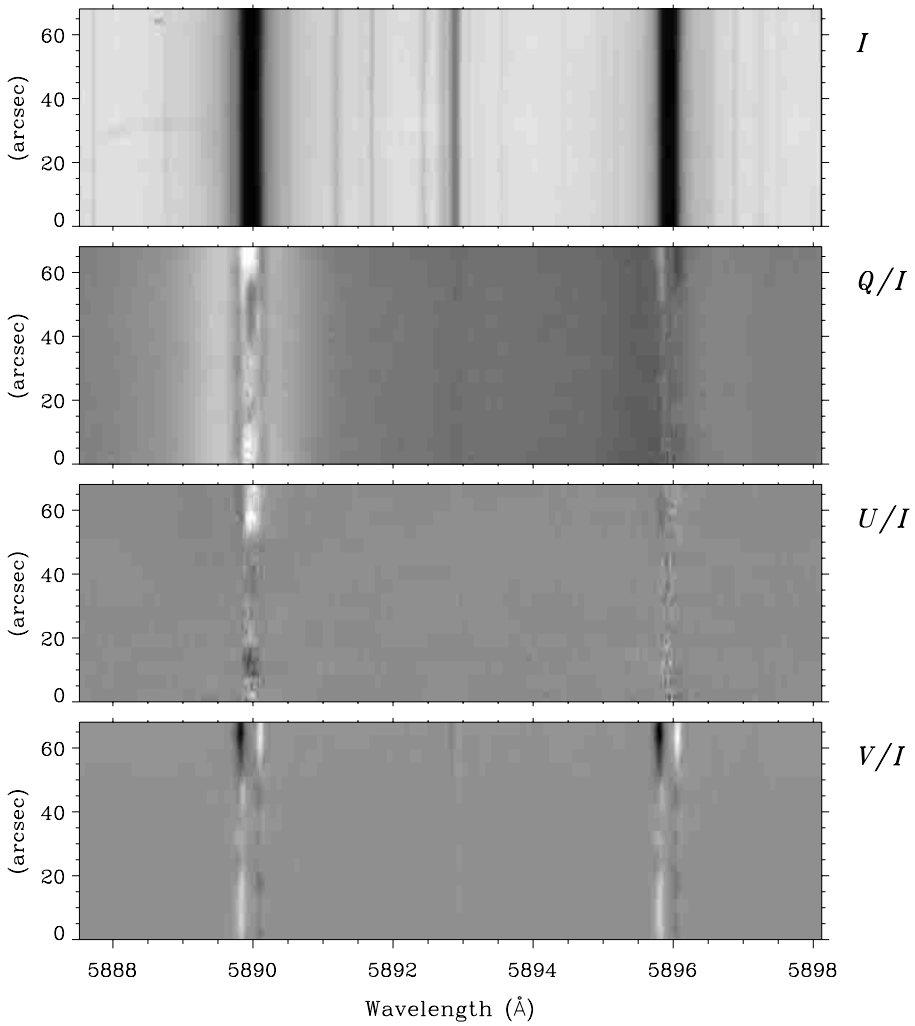

Fig. 3. Stokes spectra of a magnetic region near the SE limb at $\mu = 0.1$ like Fig. 2 but at a different position angle

must be insignificant, because there is hardly any ambiguity in the selection of the cross talk terms in the data analysis. The removal of instrumental cross talk between two of the Stokes parameters consists of adding to or subtracting from one parameter some fraction of the other. If we for instance would apply some fraction of Q/I to U/I or V/I, we would transfer some of the peculiar quantum-interference pattern in the extended wings of the Q/I profiles to appear in the U/I and V/I profiles, which would be unphysical. Similarly, the characteristic signature of the longitudinal Zeeman effect is exclusive for V/I and should not appear in Q/I or U/I. Cross talk from U/I into Q/I or V/I is not very significant here, since in most cases U/I, which is produced by Hanle rotation, has considerably smaller amplitudes than the other Stokes parameters.

4. Identification of the physical mechanisms

For each point or exposed pixel row along the slit in our 12 Stokes recordings at $\mu = 0.1$ of the Na I spectra (two of which were shown in Figs. 2 and 3) we can extract a full Stokes spectrum. This gives us a set of more than one thousand Stokes spectra (as each recording has 97 exposed pixel rows, there are $12 \times 97 = 1164$ spectra). The number of linearly independent spectra is however more like a few hundred, since the spatial step between two exposed pixel rows is 0.71 arcsec, while the effective spatial resolution was hardly better than about 2 arcsec. In any case, each of these hundreds of linearly independent spectra display a diverse and complex response to the fluctuating magnetic fields on the Sun. Together they significantly constrain the possible theories for the enigmatic D_2–D_1 polarization. We will now use this data set to try to identify the physical processes that are responsible for the core peaks. Our aim is to put the theoretical efforts on the right track.

Since Q/I, U/I, and V/I fluctuate greatly from point to point in a seemingly rather uncorrelated way, it is difficult to pick out what may be considered a "typical" magnetic-field effect. The effects depend on the three spatial directions as well as the magnitude of the field, and each of these parameters may vary spatially from point to point. We will therefore adopt a statistical approach: for each Stokes spectrum (at each spatial location) we extract a small set of well-defined profile parameters. In principle we thus get a set of 1164 combinations of these profile

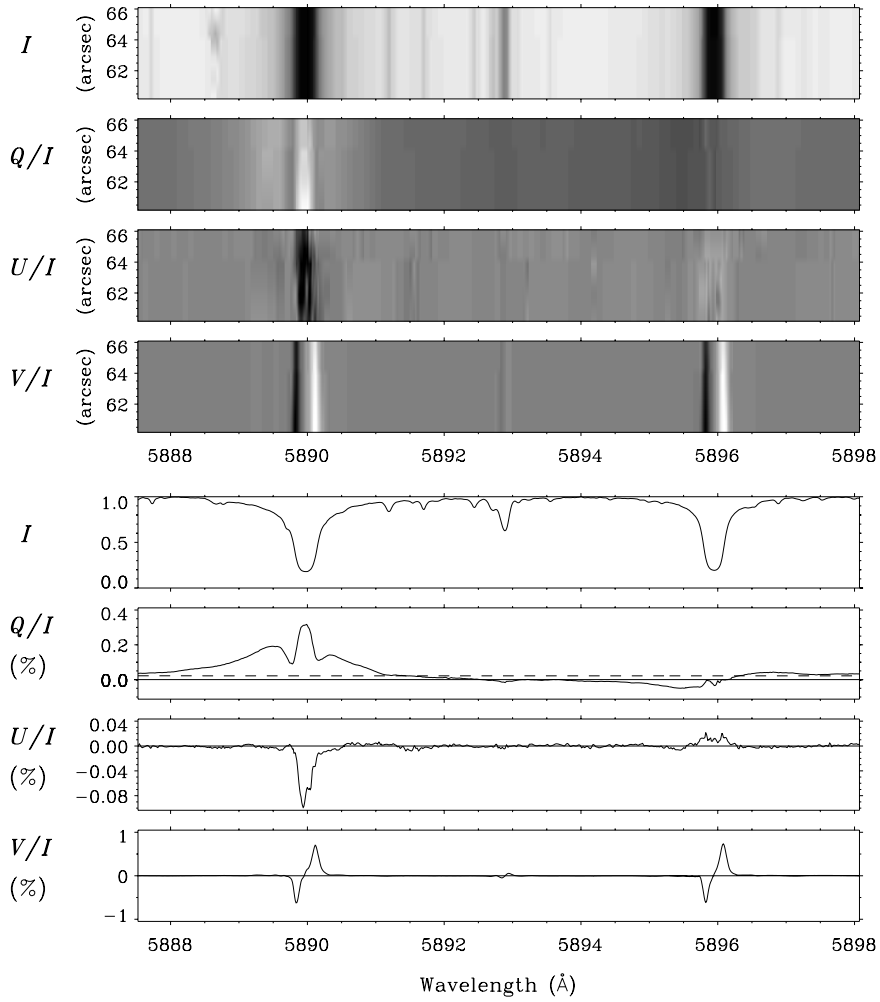

Fig. 4. Zoomed-in portion of Fig. 2, displaying the 61–66 arcsec section of the spectrograph slit. The graphical 1-D spectra in the lower part represent spatial averages over the 2-D spectra in the upper part of the figure. The dashed, horizontal line in the Q/I spectrum represent the level of the continuum polarization as determined from theory. Note the strong U/I polarization in the D_2 line and the opposite sign of U/I in D_1

parameters. For various selected pairs of parameters we can then make scatter plots and explore their distribution functions. Idealized theoretical models allow us to make corresponding synthetic scatter plots. Comparison between the empirical and theoretical distributions then guides us in a discrimination between different theoretical explanations.

The main question that we want to answer or clarify is whether the mechanism of optical depopulation pumping to produce lower-level polarization that has been proposed by Landi Degl'Innocenti (1998, 1999) is the main physical process that is responsible for the core polarization in the D_2 and D_1 lines, or whether the core peaks may be due to other processes, like partial frequency redistribution. Since the physics involved is very complex and difficult to model without great simplifications, we want to limit ourselves to the weak-field case for this comparison between observations and theory. The 12 solar regions that we have recorded at $\mu = 0.1$ cover a wide range of field strengths, from weak to intermediate or moderately strong fields, although the fields are not strong enough for the transverse Zeeman effect to show up significantly. From inspection of the data sets we find that it is useful to divide the 12 recordings in two groups, one with 9 of them, the other with the remaining 3. We will make separate scatter plots for the two groups. As we will see (Figs. 6 and 9 below) the behavior of their distributions is distinctly different. In good approximation, the group of 9 represents the weak-field case, the group of 3 the intermediate-field case, although there is some overlap between them. The recordings illustrated in Figs. 2–5 belong to the group of 3. In the group of 9 the variations are less dramatic than in these figures.

4.1. Empirical scatter plots for the weak-field recordings

We begin with the group of 9, since it is the scatter plots of this fairly homogeneous group that we want to try to model in terms of the weak-field theory. Since the Q/I

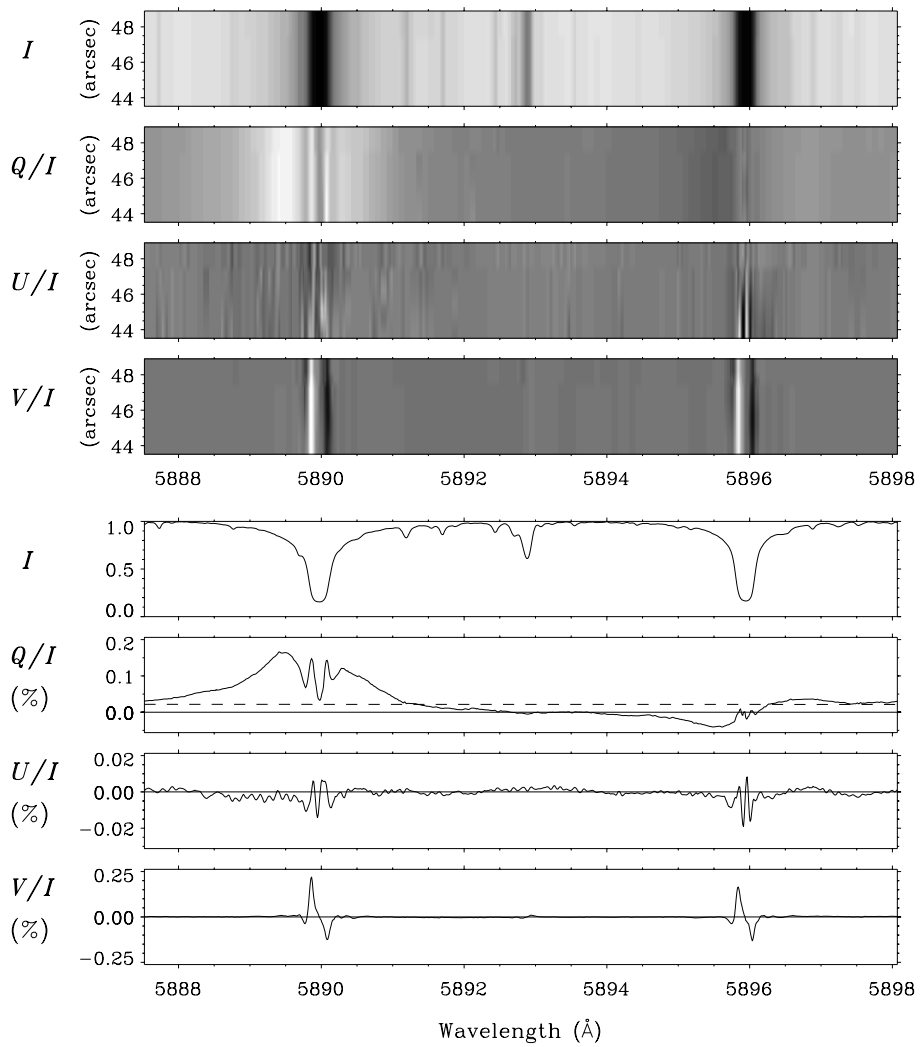

Fig. 5. Zoomed-in portion of Fig. 3, displaying the 44–49 arcsec section of the spectrograph slit. Note the complex core structure of Q/I in the D_2 Doppler core, with a pronounced polarization reversal surrounded by narrow maxima and minima

wing polarization is not affected by the Hanle effect and therefore depends almost exclusively on center-to-limb distance, it is useful to normalize all the extracted polarization values to the polarization maximum in the blue wing of the D_2 line, thereby making all the extracted parameters dimensionless, and reducing the scatter that is caused by small fluctuations in the precise limb distance for the various recordings at the nominal $\mu = 0.1$ positions. On average, the blue-wing maximum of Q/I has the value 0.2% at that limb distance.

The parameters that we have extracted for the present scatter plots are: Q/I and U/I at the centers of the D_1 and D_2 lines, the Q/I maximum in the D_2 blue wing, and the V/I signal in the D_2 line. The extracted Q/I and U/I signals are defined as the averages within 40 mÅ wide spectral windows centered at the nominal wavelengths of the D_2 and D_1 line centers and the D_2 blue wing maximum. The V/I signal is defined as $\frac{1}{2}(V_{\rm blue}/I - V_{\rm red}/I)$, where $V_{\rm blue}$ and $V_{\rm red}$ represent the extrema of the blue and red wing lobe, respectively. For small V/I amplitudes when the extrema become ill defined due to noise fluctuations, we reject the corresponding points in the scatter plots where the V signal is used. For the other scatter plots (of Q and U), all points are used.

In the panel to the upper left of Fig. 6 we have plotted the Q core polarizations in the D_1 and D_2 lines against each other. According to the investigation of the "non-magnetic" polarization of the Na I D_1 and D_2 lines in Stenflo et al. (2000a) the D_2 core polarization at $\mu = 0.1$ is 1.5 in units of the D_2 blue wing polarization, while the D_1 polarization is 0.27 of that, or 0.405 as expressed in the same, dimensionless units. Therefore we have drawn the vertical line at the abscissa value of 1.5. The top of that line is the place in the panel where the data point from Stenflo et al. (2000a) would have fallen. It can be seen as representing the case in which the Hanle effect is vanishing. In magnetic regions, due to Hanle depolarization, we expect the points to fall to the left of 1.5 and below 0.4. This is largely the case for this sample of 9 recordings.

In the panel to the lower left of Fig. 6 we have plotted the U core polarization in the D_2 line vs. the Q core polarization in the same line. For the same reasons as above

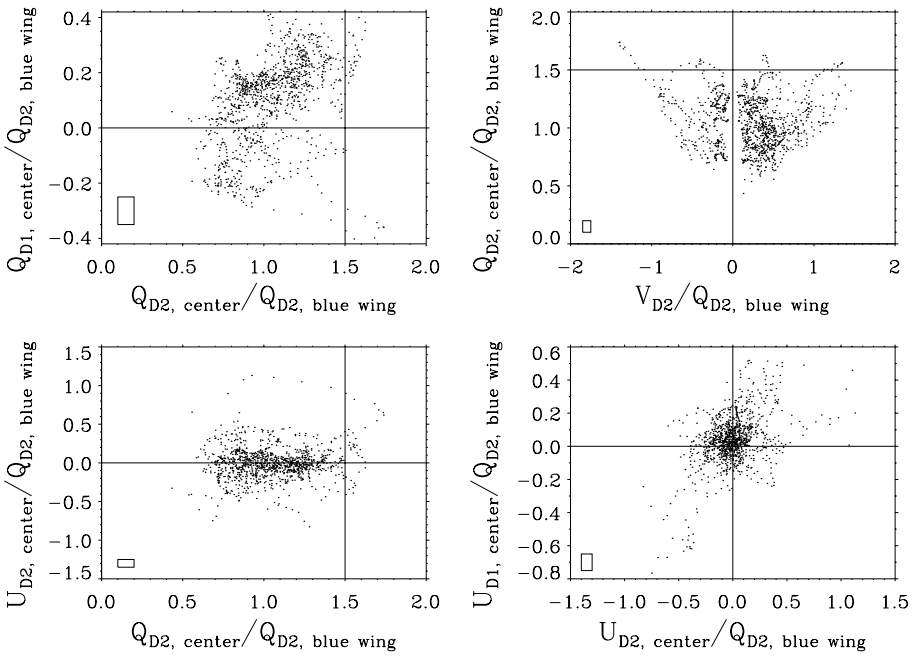

Fig. 6. Scatter plots for the 9 weak-field Stokes spectra recorded at $\mu = 0.1$. All polarization parameters are normalized in terms of the polarization amplitude in the blue wing of D_2. The estimated error boxes are given to the lower left in each panel. Upper left: Q polarization at line center in the D_1 line vs. the corresponding polarization in the D_2 line. Lower left: U vs. Q at the center of the D_2 line. Lower right: U polarization at line center in the D_1 line vs. the corresponding polarization in the D_2 line. Upper right: Q polarization at line center in the D_2 line vs. the Stokes V signal in the same line. A "zone of avoidance" is seen where the V polarization is not well defined. The lines drawn at a value of 1.5 for the Q polarization at the D_2 line core represent the non-magnetic polarization according to Stenflo et al. (2000a)

we have drawn the vertical line at 1.5. The point where it crosses the zero line should represent the case when the Hanle effect is vanishing. There is little correlation between U and Q, but this is expected since the different magnetic geometries affect the Hanle rotation and depolarization differently.

In the panel to the lower right of Fig. 6 we have plotted U at the center of the D_1 line vs. U at the center of the D_2 line. There is strikingly little correlation between U in the D_1 and D_2 lines, an unexpected result that cannot be explained by noise (since the scatter is much larger than the size of the error box).

Finally the panel to the upper right of Fig. 6 shows Q at the core of the D_2 line vs. the Stokes V signal in the same line. Here the "line of vanishing Hanle effect" is the horizontal line at 1.5. For small values of V there is a "zone of avoidance", an artificial gap in the distribution, because of rejection of points that did not satisfy the criterion for a meaningful determination of the V signal, as described above.

The estimated error box is given as the rectangle to the lower left of each panel. It has a side of 0.1 in both directions in each panel. In absolute units this corresponds to $2\ 10^{-4}$ (since the Q/I blue wing maximum in D_2, which serves as our unit, equals 0.2%). It is a fair and relatively conservative representation of the random noise. Additional error contributions may come from the cross talk corrections and the positioning of the zero line of the polarization scale.

4.2. Synthetic scatter plots for the weak-field Hanle effect

To produce synthetic scatter plots that we may compare with the empirical ones in Fig. 6 we assume that the angular distribution of field vectors is random and isotropic, that all the field strengths are in the weak-field limit in which the frequency-independent, weak-field Hanle scattering phase matrix may be used, and that it is sufficient to consider single scattering processes. Accordingly the incident radiation is entering from below in the vertical direction (approximation of extreme limb darkening) rather than being distributed over a wide cone angle centered around the vertical direction. The scattering angle is defined by the μ value at which we observe, here $\mu = 0.1$ (which is rather close to 90° scattering). For a given direction and strength of the magnetic field we can then use the weak-field Hanle phase matrix to calculate Q and U. As Stokes V is not produced by the scattering phase matrix, but is due to the longitudinal Zeeman effect regardless of scattering processes, we will deal with it separately below.

Note that we are with the present idealized model not calculating absolute polarization values (which would require full-scale radiative transfer) but *relative* fluctuations due to varying magnetic fields. The conclusions are not sensitive to the particular choice of angular distribution, for reasons that will be pointed out near the end of the present section.

Assuming that the incident radiation is unpolarized, the scattering process gives us a certain pair of Q and U values for a specified magnetic field vector. In the limit of zero magnetic field we get $Q = Q_{\rm max}$ and $U = 0$. At the line center, where the Hanle phase matrix has its validity, $Q_{\rm max}$ for D_2 is 1.5 in units of the D_2 blue wing maximum, while $Q_{\rm max}$ for D_1 is 0.27 times that value, according to the previous subsection and Stenflo et al. (2000a). Thus, after we have computed $Q/Q_{\rm max}$ and $U/Q_{\rm max}$ from the Hanle phase matrix, we can normalize these values to the D_2 blue wing maximum, to obtain the same dimensionless units as used in the empirical Fig. 6.

The field direction is represented by the azimuth angle χ_B, calculated in the counter-clockwise direction around the vertical from the plane that contains the vertical and the observer, and the colatitude θ_B, which is the angle between the field vector and the vertical. The field strength is characterised by the parameter γ_B, where

$$\gamma_B = 0.5 g\, \omega_{\rm L}\, /\Gamma\,. \qquad (1)$$

Here g is the Landé factor of the polarized atomic state, $\omega_{\rm L}$ the Larmor precession frequency, while Γ represents the decay rate (inverse life time) of the atomic state. With the atomic data for the life times and Landé factors for the excited states of the D_1 and D_2 lines, we find that $\gamma_B = 1$ when the field strength $B = 5.3$ G for the D_2 line, 10.5 G for the D_1 line. Lengthy but convenient trigonometric expressions for the dependence of the Hanle phase matrix on θ_B, χ_B, and γ_B have been given by Landi Degl'Innocenti (1988).

In contrast, the ground state has a radiative life time that is about two orders of magnitude longer than the radiative life times of the excited states, i.e., a decay rate Γ due to radiative excitation which is about two orders of magnitude smaller. This means that γ_B becomes unity already for fields of 50–100 mG due to radiative decay. Significant Hanle depolarization begins already for fields in the range of tens of mG (Landi Degl'Innocenti 1998).

Let us now consider the longitudinal Zeeman effect and Stokes V. As the Zeeman splitting is small in comparison with the width of the D_2 line, we have, with our definition of the Stokes V signal as the extremum value of V/I, and ignoring any line asymmetries,

$$\left(\frac{V}{I}\right)_{\rm max} = 4.67\ 10^{-13}\, g_{\rm eff} \lambda^2 B_{\parallel} \left[\frac{1}{I/I_{\rm c}} \frac{\partial (I/I_{\rm c})}{\partial \lambda}\right]_{\rm max}, \qquad (2)$$

where λ should be expressed in Å and the line-of-sight component of the field strength in G. The effective Landé factor is for the D_2 line $g_{\rm eff} = 1.167$. According to the previous paragraph we further have for the D_2 line

$$B_{\parallel} = 5.3 \gamma_B \cos b \ {\rm G}\,, \qquad (3)$$

where b is the angle between the magnetic field and the line of sight. If θ is the angle between the line of sight and the vertical direction, simple spherical trigonometry gives

$$\cos b = \cos\theta \cos\theta_B + \sin\theta \sin\theta_B \cos\chi_B\,. \qquad (4)$$

The intensity gradient can be evaluated from previous ZIMPOL recordings. We find that the maximum of $g_{\rm eff}|\partial I/\partial\lambda|/I$ is 18.9 for the D_2 line. V/I can be converted from absolute polarization units to be expressed in units of the Q/I maximum of the blue wing of the D_2 line, as we did for the line-center values of Q and U.

With the above set of equations we can derive, with θ_B, χ_B, and γ_B as input (direction and strength of the magnetic field), the Stokes V signal in the D_2 line expressed in the same dimensionless units as used for the empirical scatter plots. The same input values are used to derive all the other Q and U profile parameters used in the scatter plot diagrams.

Each combination of the three input parameters θ_B, χ_B, and γ_B gives us one point in each of the four scatter-plot panels. To obtain a distribution of points we have to assume some distribution of field vectors. To produce a set of four scatter-plot diagrams from a given model we will assume a fixed value for the field strength and assume that the fixed-size field vectors have an isotropic distribution. For this purpose we divide up the unit sphere that represents the $\chi_B - \theta_B$ space in boxes with equal area. This is achieved with a grid that is equidistant in $\cos\theta_B$ and in χ_B. It is the same procedure that we used to produce theoretical Hanle histograms in Bianda et al. (1998b), so we refer to this paper for more technical details.

Let us now apply this idealized theory to compute scatter plots for some different model cases and compare with the empirical scatter plots in Fig. 6. We assume in the following that the field strength is kept fixed at 3.7 G, since this choice produces reasonable distributions and is consistent with previous Hanle investigations (Bianda et al. 1998a,b, 1999). A variation of this assumption is discussed later.

The first case that we consider is what the situation would be, if the theory of Landi Degl'Innocenti (1998, 1999) were correct in the sense that *both* the D_1 and D_2 core peaks in Q/I are due to lower-level atomic polarization produced by optical depopulation pumping. In this case, due to the very long life time of the lower (ground) state, $\gamma_B \gg 1$ for both the D_1 and D_2 lines, which means that we are in the Hanle saturated regime for both lines. In this "strong-field limit" of complete Hanle saturation we obtain the scatter plots of Fig. 7. (We have here used $\gamma_B = 35$ and 70 for the D_1 and D_2 lines, respectively, but any larger values would result in the same scatter plots, since in this regime the Hanle effect is decoupled from the field strength.) The most important property of these scatter plots is that the D_2 and D_1 lines are fully correlated, since both belong to the same field-strength regime. This leads to the well-defined straight-line relations between $Q_{\rm D1}$ and $Q_{\rm D2}$ on the one hand (panel to the upper left) and $U_{\rm D1}$ and $U_{\rm D2}$ on the other hand (panel to the lower right). In the remaining two panels the points scatter over a substantial area, because Q, U, and V are only weakly correlated with each other. The special non-random pattern arises from the way in which the field orientations were selected from the grid on the unit sphere.

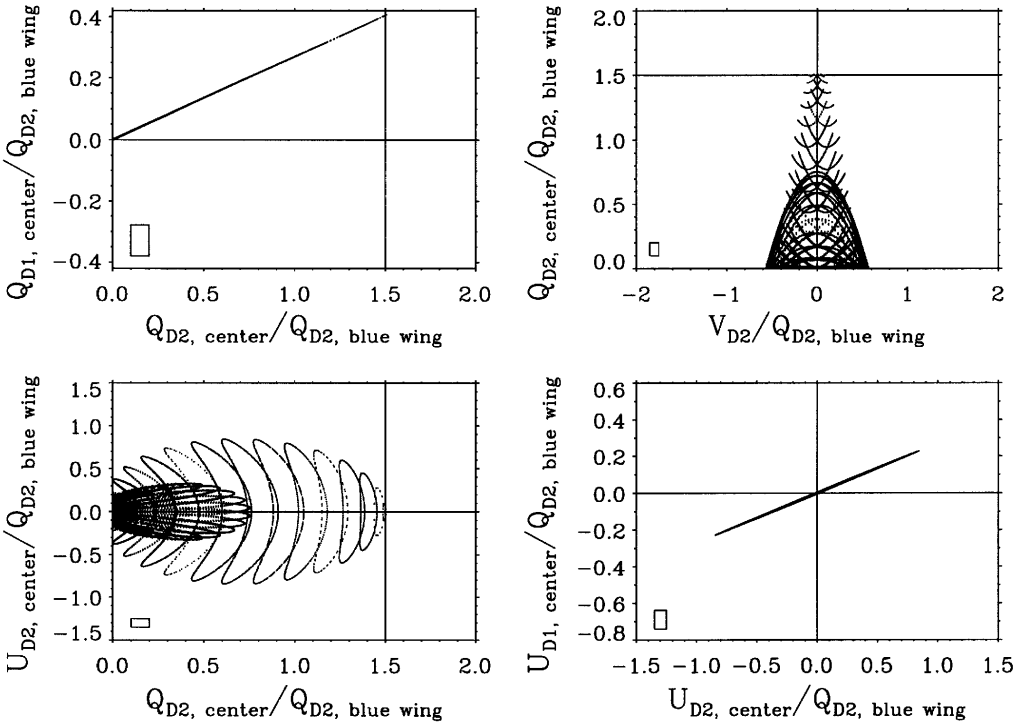

Fig. 7. Synthetic scatter plots based on the assumption that both the D_2 and D_1 line polarizations are governed by lower-level atomic polarization produced by optical depopulation pumping. Both lines are in the saturated (strong field) Hanle regime because of the long life time of the atomic ground state. The field vectors are assumed to have an isotropic distribution

Although the angular distribution is isotropic, the points on the unit sphere have been picked from a fixed grid and not a random distribution, and this leads to the particular fixed pattern in the scatter plots, which in a more realistic, Monte Carlo simulation would be smoothed out.

It is interesting to note that all polarization is not destroyed by Hanle depolarization, even in the limit of strong magnetic fields (i.e., $\gamma_B \gg 1$), since the amount of depolarization is angle dependent. For a vertical magnetic field, in which case the illumination of the scattering particle is symmetric around the field vector, there is no depolarization at all, regardless of the field strength. The depolarization becomes complete if the magnetic field is oriented along the line of sight. For other orientations the depolarization is partial.

In the strong-field regime the Hanle effect gets decoupled from the field strength or γ_B and depends only on the orientation (angles θ_B and χ_B). This angular dependence is identical for the D_1 and D_2 lines. Since in the model that we have described the polarization in both line cores are governed by ground-state atomic polarization as proposed by Landi Degl'Innocenti (1998, 1999), both lines are decoupled from the field strength and depend on the field orientation in the same way. This is the reason for the perfect correlation between the two lines in the upper left and lower right panels of Fig. 7. Such a correlation is not at all seen in the observational scatter plots of Fig. 6.

Let us now introduce a different model, for which the core polarization in the D_2 line is governed by the atomic polarization induced by the incident radiation field in the excited state of the D_2 transition instead of by lower-level polarization. For the D_1 line, however, we keep our previous model assumption that this line is exclusively governed by ground-state atomic polarization acquired by the process of optical depopulation pumping, since there is presently no known way to produce D_1 core polarization in any other way. In this new model the D_2 and D_1 lines belong to two entirely different Hanle regimes. While the D_2 line is in the middle of its sensitivity range for typical solar field strengths at the height of line formation, the D_1 line remains in the strong-field, Hanle saturated regime. Due to the difference of the regimes, the behavior of the two lines will be much less correlated than before.

Since the upper, $J = \frac{3}{2}$ state of the D_2 transition is indeed polarizable, in contrast to the upper, $J = \frac{1}{2}$ state of the D_1 transition, and since the D_2 line has a polarizability factor W_2 as large as 0.5 in the absence of any ground-state polarization, there is no compelling need to invoke optical depopulation pumping and lower-level polarization in the case of the D_2 line. For the D_1 line on the other hand we have presently no other choice than to invoke lower-state polarization. It is therefore not unnatural that the D_2 and D_1 lines could belong to widely different Hanle regimes.

For a given field strength, the value of the parameter γ_B depends on the value of Γ/g for the atomic level responsible for the polarization, according to Eq. (1). If the excited state rather than the ground state of the D_2 transition is responsible for the core polarization that we

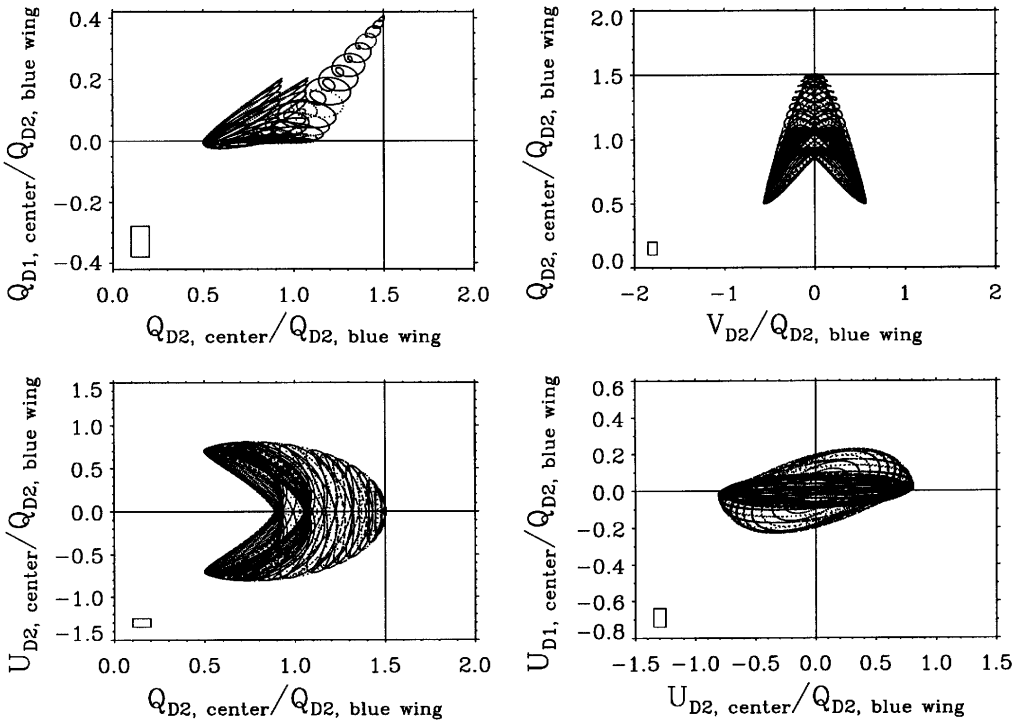

Fig. 8. Synthetic scatter plots based on the assumption that only the D_1 line polarization is governed by lower-level atomic polarization produced by optical depopulation pumping, while the D_2 polarization is governed by the atomic polarization in the excited state. The D_1 and D_2 lines then belong to entirely different Hanle regimes. The magnetic field is assumed to have a strength of 3.7 G and an isotropic angular distribution

observe in the D_2 line, then a field strength of 3.7 G corresponds to $\gamma_B = 0.70$ for that line.

Thus assuming that $\gamma_B = 0.7$ for the D_2 line and that $\gamma_B \gg 1$ (we have used $\gamma_B = 35$, but a much larger value would give the same result) for the D_1 line, then we obtain the scatter plots shown in Fig. 8. Now we see how the separation of the regimes makes the two lines more uncorrelated and leads to rather broad point distributions in all the panels. Note that slightly negative values of the D_1 core polarization occurs in the panel to the upper left as we use $\mu = 0.1$ (rather than 0.0).

Complete Hanle depolarization can only occur for $\gamma_B \gg 1$. Since γ_B is only moderately large (0.7) for the D_2 line, the depolarization is only partial, even when the magnetic field vector is along the line of sight.

When we now compare the synthetic scatter plots in Fig. 8 with the empirical ones in Fig. 6, we find a reasonably good agreement, even surprisingly good in view of the drastic idealizations made in the model, like single-valued field strength, single scattering corresponding to extreme limb-darkening, no radiative transfer, and polarization governed exclusively by the Hanle weak-field phase matrix. The distributions broaden considerably in a non-linear way when we go to larger μ values, so it is likely that the distributions would be modified and broadened if we would integrate over a wide cone angle of the incident radiation field. Further broadening would occur if we would introduce a distribution of field strengths in the model. The Hanle effect is likely to couple to partial frequency redistribution effects in vector radiative transfer. The D_2 core polarization may not be exclusively due to upper-state atomic polarization, but the lower-state polarization may also have a mixed-in effect for the D_2 line. All of these questions represent challenging tasks for future theoretical explorations.

The particular choice of $\gamma_B = 0.7$ for the D_2 line has been made to crudely optimize the similarity to the empirical scatter plots. The chosen value of γ_B governs the spread of the D_2 polarization values. If γ_B were significantly larger, the regions where the dimensionless values on the horizontal axes in the scatter plot panels to the upper and lower left (or on the vertical axis of the panel to the upper right) are less than 0.5 would become populated, in contradiction with the observed distributions in Fig. 6. Similarly, if γ_B were significantly smaller than 0.7, then these values would be more clustered to the 1.5 line and the spread would be smaller than in the observed scatter plots. We therefore see how the spread of the points can be used as a rather sensitive indicator of the field strength (within the framework of the present model, assuming a single-valued field). This leads to a value of 4 G, consistent with Hanle determinations in other spectral lines, like Ca I 4227 Å and Sr II 4078 Å (Bianda et al. 1998a,b, 1999).

Let us next consider how different choices for the angular distribution of field vectors would affect the results. The more we concentrate the distribution around the vertical direction, the smaller the Hanle effect will be, and the point scatter will cluster closer to the singular points

of zero magnetic field in the four diagrams of Fig. 6. The observed large scatter is only possible if a substantial fraction of the fields are highly inclined. If instead all the fields were confined to a horizontal plane, then the distribution in the diagram to the upper left of Fig. 6 would be detached from the vertical line in the diagram, with a gap between the cluster of points and the vertical line. This case cannot be fully ruled out with the present data set, but it has no influence on our conclusions concerning the two different Hanle regimes for the D_1 and D_2 lines.

Let us briefly discuss also the hypothetical case that not only the D_2 but also the D_1 core polarization is determined by atomic polarization in the excited state rather than by the ground-state polarization, although there is no theory to back up this assumption in the case of the D_1 line. In this case, if we like before assume a field strength of 3.7 G, for which γ_B has the value 0.7 for the D_2 line, we would have $\gamma_B = 0.35$ for the D_1 line (since Γ/g differs by a factor of two for the $J = \frac{3}{2}$ and $\frac{1}{2}$ excited states). If γ_B were the same for the two lines, then the points in the panels to the upper left and lower right of the scatter plot diagrams would fall along straight lines and be perfectly correlated, as they were in Fig. 7. As the values of γ_B differ by a factor of two, there will be some spread around these straight-line relations, but the spread will be quite small, because the two γ_B values do not differ enough but belong to the same Hanle regime. Therefore this hypothetical model case is inconsistent with the empirical scatter plots. The lack of strong, empirical correlation between the core polarizations in the two lines can only be given a consistent explanation if the two lines belong to vastly different Hanle regimes, as they do for the model of Fig. 8.

4.3. Empirical scatter plots for the intermediate-field recordings

When considering the comparison between the synthetic scatter plots in Fig. 8 with the empirical ones in Fig. 6 we need to remember the smoothing effect by the error boxes, which may be somewhat underestimated if there are systematic error contributions from cross talk and zero line corrections. An additional factor is that the set of spatial regions sampled on the Sun by the spectrograph slit may not be that homogeneous but could include not only a range of various field strengths, but also fields that lie outside the range of validity of the weak-field approximation for the Hanle phase matrix.

From the 12 solar regions recorded at $\mu = 0.1$, a group of 9 was selected for the scatter plots in Fig. 6, since the remaining 3 recordings exhibited more dramatic magnetic-field effects likely to be outside the weak-field range, as mentioned in the introductory part of Sect. 4 and shown in Figs. 2–5. To illustrate this point we show in Fig. 9 the empirical scatter plots for this group of 3 recodings with fields in the intermediate range, in which scattering polarization still dominates over the transverse Zeeman effect in the Stokes Q and U parameters, while the weak-field Hanle theory is of no or doubtful validity. We indeed see how the points in Fig. 9 spread over regions far beyond those covered by the spread of points in Fig. 6.

We have no theory to describe this rather individualistic behavior of the different solar regions. However, Fig. 9 illustrates how important it is to have a sufficiently homogeneous sample of solar regions in order to arrive at a meaningful theoretical interpretation based on statistical characteristics and distributions. If some spatial points representing such intermediate-strength fields would be mixed in with our previous sample of 9 weak-field solar regions, they may significantly contribute to the scatter. In particular the occurence of negative values for the Q polarization in the D_1 line, as seen in Fig. 6, might be explained this way, since they are more frequent than the positive values in the panel to the upper left in Fig. 9. It is an interesting theoretical challenge to explain how this negative D_1 polarization can be produced.

4.4. Stokes V asymmetries

The Stokes V signals are generated by the longitudinal Zeeman effect, regardless of whether the spectral line is formed by scattering processes or not. Although the present paper focuses on the physical nature of the scattering polarization and the Hanle effect in the Na I D_1 and D_2 lines, we have seen in Figs. 6–8 that the V signal also contributes to constrain this problem, because the geometry and strength of the magnetic field governs both the Hanle effect in Q and U and the Zeeman effect in V.

Further constraints on the atmospheric structure, dynamics, and field geometry are provided by the detailed properties of the shapes of the Stokes V profiles, in particular by the Stokes V asymmetries (Stenflo et al. 1984). These asymmetries are signatures of strong gradients in the magnetic and velocity fields. The most favorable conditions for the appearance of large asymmetries occur when the magnetic and flow fields are spatially separated with a magnetopause structure, e.g. a flux tube wall or a magnetic canopy, which separates the stronger magnetic field region from a weaker or field-free one (Grossmann-Doerth et al. 1988, 2000; Steiner 2000). Sigwarth et al. (1999) have recently explored the statistical properties and distributions of the Stokes V amplitude and area asymmetries as measured with good spatial resolution in the Fe I 6302 Å line, and explored their correlations with various other line parameters extracted from the Stokes I and V profiles.

The amplitude asymmetry δa is defined as

$$\delta a = \frac{V_{\rm blue} + V_{\rm red}}{V_{\rm blue} - V_{\rm red}}\,, \tag{5}$$

where $V_{\rm blue,\,red}$ represents the Stokes V amplitude with sign. Similarly we define the area asymmetry if we instead let $V_{\rm blue,\,red}$ represent the areas of the blue and red wing lobes of Stokes V. Positive (negative) asymmetry means predominance of the blue (red) lobe. An asymmetry of $+1$ or -1 means a single-lobe profile, while values larger

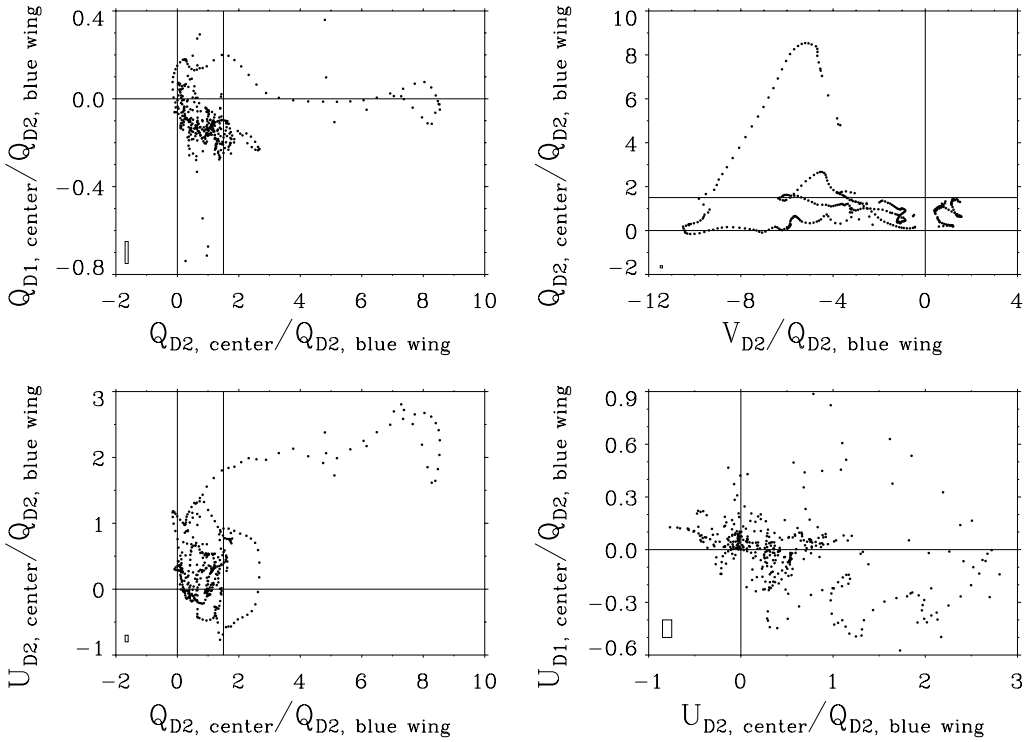

Fig. 9. Scatter plots for the 3 Stokes spectra recorded at $\mu = 0.1$, which represent much stronger magnetic fields than the corresponding scatter plots for the group of 9 weak-field spectra that were shown in Fig. 6. The notations are the same as in that figure

than +1 or smaller than −1 represent the "pathological" case when both lobes have the same sign. For a theoretical parameter survey of these various cases, see Steiner (2000).

We have determined the V/I amplitude asymmetries of the D_2 and D_1 lines for our recordings at $\mu = 0.1$ and examined their distributions. At this small limb distance these strong lines should be formed in the lower chromosphere, where we may expect magnetopause stratifications in the form of magnetic canopies overlying the weaker-field regions, with different flow fields above and below the canopy interfaces.

Since the asymmetries determined in the D_2 and D_1 lines are found to be almost the same (within the error bars), we here only illustrate the distributions for the D_2 line. In Fig. 10 the thick, solid line shows the histogram of the V/I amplitude asymmetries δa_{D2} for the group of 9 weak-field recordings that were used for the scatter plots in Fig. 6, while the dotted histogram represents the group of 3 stronger-field regions used for the scatter plots in Fig. 9 and the illustrations in Figs. 2–5.

It is particularly striking that the group of weaker-field regions has a much broader distribution than the stronger-field regions. About 40% of the asymmetries have values $|\delta a_{D2}| > 1$, which corresponds to "pathological" two-humped V/I profiles with the same signs for the blue and red lobes. In his theoretical survey Steiner (2000) clarifies how such profiles are produced under conditions for the gradients of the temperature, velocity, and magnetic field which may be expected to occur in the lower chromosphere, where the D_2 and D_1 lines are formed. The diagnostic information provided by V/I is different from and highly complementary to the information and constraints obtained from Q/I and U/I.

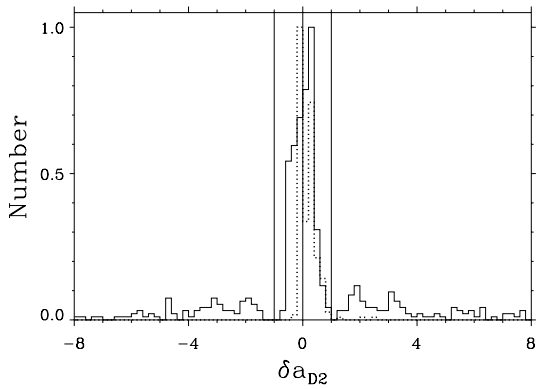

Fig. 10. Histograms for the Stokes V/I amplitude asymmetries in the D_2 line, normalized to a maximum value of unity. The thick, solid curve represents the distribution for the group of 9 weak-field regions used for the scatter plots in Fig. 6, while the dotted histogram represents the group of 3 stronger-field regions used for the scatter plots in Fig. 9. The asymmetry values −1, 0, and +1 are marked by thin vertical lines. The region $|\delta a| > 1$ corresponds to two-humped profiles (meaning that the blue and red V/I lobes have the same sign)

5. Concluding discussion

The discovery of the enigmatic and unexpected Q/I core polarization peaks in the Na I D_1 and D_2 lines (Stenflo & Keller 1996, 1997) and the theoretical explanation

proposed by Landi Degl'Innocenti (1998, 1999) have led to a new, intriguing paradox for the Sun: How can ground-state atomic polarization needed to explain the D_1 core polarization sufficiently survive destruction by the ubiquitous magnetic fields in the solar atmosphere? Due to the very long life times of atomic ground states, effects of Hanle depolarization would set in already for magnetic fields in the mG range. The existence of such weak fields in the highly conductive and dynamic solar plasma is hard to imagine on theoretical grounds and also seems to be excluded by other Hanle and Zeeman observations.

The Hanle depolarization effects however depend not only on field strength but also on field direction. Thus the ground-state polarization can avoid destruction if the field is sufficiently vertical with respect to the solar surface. A nearly vertical field could provide a solution to the paradox, although it seems to contradict the commonly held view that the magnetic fields in the lower chromosphere, where the D_1 and D_2 line cores are formed, are predominantly horizontal with a canopy structure. We have here presented observations that try to resolve this paradox, by exploring the influence of magnetic fields on the scattering polarization and examining the resulting statistical distributions of the Hanle-effect signatures.

As such a program requires full vector polarimetry we could only embark on it when ZIMPOL II, the second generation of our imaging polarimeter system, became available. ZIMPOL II was used for the first time for a science program at NSO/Kitt Peak during two observing runs in October 1999 and March 2000. Many different spectral regions were recorded, but priority was given to explore the Na I D_1 and D_2 paradox. To eliminate effects of center-to-limb distance we have selected for the present analysis the set of recordings that were all made at the same limb distance (but at different position angles), corresponding to $\mu = 0.1$.

Statistical analysis shows that the Hanle Q/I and U/I signatures in the D_1 and D_2 lines are quite uncorrelated with each other, which suggests that the core polarizations in the two lines belong to very different Hanle regimes. This is the case if lower-level atomic polarization is only responsible for the D_1 core polarization but plays an insignificant or subordinate role for the D_2 line. This conclusion is supported by the similarity between the empirical scatter plots and the synthetic ones computed with the assumption of a 3.7 G magnetic field with an isotropic angular distribution under the assumption that the Hanle depolarization is governed by the life time of the excited atomic state for the D_2 line and the life time of the ground state for the D_1 line. It indicates that the theory of Landi Degl'Innocenti (1998, 1999) is correct for the D_1 line, but that it is of relatively small relevance for the D_2 line.

It follows from this resolution of the Na I line paradox that a larger fraction of the magnetic fields than previously believed must be nearly vertical. In the magnetic limb regions that we have studied here, and which have varying degrees of facular activity, an angular distribution similar to an isotropic one seems to provide a sufficient fraction of nearly vertical fields to explain the observations. In comparison, for our previous observations of the "second solar spectrum" with ZIMPOL I, which were always carried out in the most quiet and field-free regions that we could find, a much larger fraction of the field vectors must be "nearly vertical" to explain the observations. Thus, in our studies of the detailed center-to-limb variation of the D_1 and D_2 polarization (Stenflo et al. 2000a), we consistently found prominent core peaks in the D_1 line, which with the lower-level polarization theory could only exist either if the field were nearly vertical (without any restriction on the field strength), or if it were weaker than about 10 mG. Having this choice, a vertical orientation appears much more plausible than an ultraweak field strength. This leads to the rather surprising conclusion that the magnetic field in the lower chromosphere is preferentially vertical in the most quiet solar regions.

In our construction of synthetic scatter plots we have implicitly assumed that the magnetic field is spatially resolved. Each computed point is based on a well defined strength and direction of the field. Another limiting model case would be the so-called microturbulent limit, when all magnetic elements are assumed to be optically thin, and we average over a distribution of field vectors along the line-of-sight range of formation of the spectral line. In this case we would expect to find substantial Hanle depolarization (in Q/I) but little or no Hanle rotation (in U/I), since Hanle rotation can give signatures of both signs, which leads to cancellation effects in the averaging process, while Hanle depolarization should at least nominally have only one sign. The observed relative amount of scatter in the U and Q parameters supports the view that most of the Hanle signatures that we have observed in our selected set of magnetic regions are indeed largely spatially resolved, otherwise we would expect the relative amount of scatter in U to be smaller.

Since the D_2 line is, according to atomic physics, polarizable without the help of lower-level atomic polarization (in contrast to the D_1 line), the main question for D_2 is to explain why its Q/I profile shape usually has a triplet structure. We believe that this structure is primarily a result of partial frequency redistribution (PRD) processes in vector radiative transfer, like the explanation for the similar Q/I triplet structure of the Ca I 4227 Å line (Rees & Saliba 1982; Saliba 1985). Test calculations by D. Fluri (private communication) support this view, but this complex problem needs to be explored much more.

In his attempt to explain the D_1 and D_2 core polarization, Landi Degl'Innocenti (1998, 1999) avoided radiative transfer by using an idealized and parametrized model. A self-consistent, quantitative determination of the lower-level atomic polarization requires the solution of the statistical equilibrium equations with coherences in a realistic model atmosphere, which is a major challenge for future theoretical work, even in the absence of magnetic fields. For quantitative modelling of the profile shapes of the present data set we need to do such calculations with PRD and for various strengths and configurations of the

magnetic field. Since this daunting problem is unlikely to be solved in its entirety within the next couple of years, we must, for the time being, in the interpretations use various degrees of idealizations and approximations.

Diagnostically the Hanle and Zeeman effects are highly complementary to each other. While the Zeeman effect gets its major contributions from the kG flux tubes, the Hanle effect is almost "blind" to these flux tubes, mainly because of their small filling factors, but also because they prefer to be vertically oriented. The Hanle effect responds primarily to the weak fields between the flux tubes, mainly because they represent the dominating filling factor, while the Zeeman effect is almost "blind" to these fields because of their weakness. The Hanle effect can be used with advantage for strong, chromospheric lines, while the Zeeman effect works much better for photospheric lines.

Since the Hanle effect only occurs as a magnetic-field induced modification of polarization produced by coherent scattering, it can never be treated by any LTE approximation. As a polarized non-LTE scattering problem, it couples the 3-D magnetized atmosphere over regions of optical thickness unity, where the sources of the incident, anisotropic radiation field are located. Eventually one would like to take some MHD model produced by extensive numerical simulation of magnetoconvection and use it to calculate synthetic maps of the Hanle and Zeeman signatures in various spectral lines and at various center-to-limb distances, in order to test such simulation models against Stokes observations. This task requires efficient numerical algorithms for 3-D polarized radiative transfer with coherences and PRD in arbitrary magnetized atmospheres. It is a long-term goal that we try to approach step by step.

Acknowledgements. We wish to thank the engineering group at ETH Zurich (Peter Povel, Peter Steiner, Urs Egger, Frieder Aebersold), who built the ZIMPOL system and provided the technical support. Peter Povel took part in the October 1999 observing run, Urs Egger in the March 2000 run. The ZIMPOL development program and one of us (A.G.) have been funded by the Swiss Nationalfonds, grant No. 20-50464.97/1. The National Solar Observatory, where the observations were done, is one of the National Optical Astronomy Observatories, which are operated by the Association of Universities for Research in Astronomy, Inc. (AURA) under cooperative agreement with the National Science Foundation.

References

Bianda, M., Solanki, S.K., & Stenflo, J. O. 1998a, A&A, 331, 760
Bianda, M., Stenflo, J. O., & Solanki, S. K. 1998b, A&A, 337, 565
Bianda, M., Stenflo, J. O., & Solanki, S. K. 1999, A&A, 350, 1060
Fluri, D. M., & Stenflo, J. O. 1999, A&A, 341, 902
Gandorfer, A. 1999, Opt. Eng., 38, 1402
Gandorfer, A. 2000, The Second Solar Spectrum, vol. I: 4625 Å to 6995 Å, ISBN no. 3 7281 2764 7 (Zurich: VdF)
Gandorfer, A., & Povel, H. 1997, A&A, 328, 381
Giovanelli, R. G. 1980, Solar Phys., 68, 49
Gisler, D. 1999, Diplomarbeit, Inst. Astron., ETH Zurich
Grossmann-Doerth, U., Schüssler, M., & Solanki, S. K. 1988, A&A, 206, L37
Grossmann-Doerth, U., Schüssler, M., Sigwarth, M., & Steiner, O. 2000, A&A, 357, 351
Jones, H. P., & Giovanelli, R. G. 1983, Solar Phys., 87, 37
Landi Degl'Innocenti, E. 1988, A&A, 192, 374
Landi Degl'Innocenti, E. 1998, Nature, 392, 256
Landi Degl'Innocenti, E. 1999, in Proc. 2nd SPW, Solar Polarization, ed. K. N. Nagendra, & J. O. Stenflo, ASSL, 243 (Dordrecht: Kluwer), 61
Omont, A., Smith, E. W., & Cooper, J. 1973, ApJ, 182, 283
Povel, H. P. 1995, Opt. Eng., 34, 1870
Rees, D. E., & Saliba, G. J. 1982, A&A, 115,1
Saliba, G. J. 1985, Solar Phys., 98, 1
Sigwarth, M., Balasubramaniam, K. S., Knölker, M., & Schmidt, W. 1999, A&A, 349, 941
Steiner, O. 2000, Solar Phys., 196, 245
Stenflo, J. O. 1980, A&A, 84, 68
Stenflo, J. O. 1994, Solar Magnetic Fields – Polarized Radiation Diagnostics (Dordrecht: Kluwer)
Stenflo, J. O. 1998, A&A, 338, 301
Stenflo, J. O. 1999, in Proc. 2nd SPW, Solar Polarization, ed. K. N. Nagendra, & J. O. Stenflo, ASSL, 243 (Dordrecht: Kluwer), 1
Stenflo, J. O, & Keller, C. U. 1996, Nature, 382, 588
Stenflo, J. O, & Keller, C. U. 1997, A&A, 321, 927
Stenflo, J. O., Baur, T. G., & Elmore, D. F. 1980, A&A, 84, 60
Stenflo, J. O., Twerenbold, D., Harvey, J. W., & Brault, J. W. 1983, A&AS, 54, 505
Stenflo, J. O, Harvey, J. W., Brault, J. W., & Solanki, S. K. 1984, A&A, 131, 33
Stenflo, J. O, Keller, C. U., & Povel, H. P. 1992, LEST Foundation Technical Report No. 54, Univ. Oslo
Stenflo, J. O, Gandorfer, A., & Keller, C. U. 2000a, A&A, 355, 781
Stenflo, J. O, Keller, C. U., & Gandorfer, A. 2000b, A&A, 355, 789
Wenzler, T. 2000, Diplomarbeit, Inst. Astron., ETH Zurich